ELSEVIER

Chemical Engineering Journal 121 (2006) 27–35

Chemical Engineering Journal

www.elsevier.com/locate/cej

Time–frequency investigation of different modes of bubble flow in a gas–solid fluidized bed

Srdjan Sasic, Bo Leckner, Filip Johnsson *

Department of Energy and Environment, Chalmers University of Technology, Hörsalsvägen 7, S-412 96 Göteborg, Sweden

Received 1 April 2005; received in revised form 16 February 2006; accepted 3 May 2006

Abstract

Three modes of bubble flow in fluidized beds, identified and explained in a previous work (S. Sasic, F. Johnsson, B. Leckner, Interaction between a fluidized bed and its air-supply system: some observations, Ind. Eng. Chem. Res. 43 (2004) 5730–5737), are studied here by linear methods (wavelet analysis) in the time–frequency plane. The modes are: (1) single bubble regime characterized by the presence of one bubble at a time in the bed; (2) a regime where single bubbles still dominate the flow field, but another type of structure (so-called exploding bubbles) becomes significant at a different frequency; (3) a regime in which exploding bubbles, conceived as gaseous structures stretching from the air distributor to the surface of the bed, clearly dominate the flow field, but pressure waves, originating from single bubbles in the bed, are still observed. The signals representing single bubbles, exploding bubbles and pressure waves are extracted from the original pressure signals by discrete wavelet analysis. These phenomena are identified as distinct local maxima in the distribution of energy over wavelet scales in a wavelet energy spectrum (obtained by statistical analysis of wavelet coefficients). Also, a model, treating the data recorded as an organized event (e.g. bubbles) and an accompanying white noise process, is used for calculation of the time scales of phenomena present in the bed in a certain fluidization situation. It is shown how these phenomena are localized in time.

Keywords: Fluidized beds; Pressure fluctuations; Wavelet analysis; Modes of bubble flow; Wavelet energy spectrum; Time scales

1. Introduction

The most commonly studied quantities in dynamic analyses of gas–solids fluidized beds are pressure fluctuations [1–5]. Although measurements of pressure fluctuations are easy to perform, the interpretation of such signals is not straightforward. It is generally accepted that the fluctuations come from bubble motion within the bed, but the exact origin of the fluctuations is usually not clear. The information present in pressure time series recorded in gas–solid fluidized beds may be revealed either by linear or nonlinear methods. Among the linear methods, amplitude analysis (the study of how the amplitude of pressure fluctuations is affected by the operating conditions of the bed) and spectral analysis (the description of the signal in the frequency domain) clearly dominate the present literature [4–6]. These methods of time series analysis are based on the crucial assumption that the signals are considered stationary (or that they may be reduced to stationarity by some simple transformation, see ref. [7]). In the literature related to pressure signals recorded in fluidized beds, the validity of such an assumption has received little attention. However, He et al. [8] demonstrated pronounced nonstationary features in fluidized beds pressure signals using a Wigner distribution (a quadratic time–frequency representation of a signal, see ref. [9]). Therefore, they presumed that no reliable information regarding the dynamics of fluidized beds can be obtained by classical Fourier analysis (spectral analysis). The interest of dealing with possible time-varying properties of signals has led to the increased use of time–frequency signal representations, designed to yield a potentially more revealing picture of the temporal localization of a signal's spectral components. The most common representations of this kind are the short-time Fourier transform and especially the wavelet transform. Wavelet transform techniques are nowadays extensively used in many fields of research: signal processing and denoising (e.g. ref. [10]), fractal analysis (e.g. ref. [11]), in fluid mechanics for the identification of coherent structures in turbulent flows (e.g. ref. [12]), image coding [13], etc. In the area of gas–solid flows, fluidization has been treated by wavelet analysis

* Corresponding author. Tel.: +46 31 772 1449; fax: +46 31 772 3592.
E-mail address: filip.johnsson@me.chalmers.se (F. Johnsson).

1385-8947/$ – see front matter © 2006 Elsevier B.V. All rights reserved.
doi:10.1016/j.cej.2006.05.005

Nomenclature

a	dilation (scaling) parameter, Eq. (1)
b	translation (location) parameter, Eq. (1)
a_0, b_0	discretization factors for scaling and location parameters, respectively
CW$f(t)$	continuous wavelet transform coefficients, Eq. (1)
DW$f(t)$	discrete wavelet transform coefficients, Eq. (2)
$D_{SC}^{(m)}$	scaled wavelet coefficients at scale m
e_m	part of the total variance of the signal, attributed to scale m, Eq. (4)
e_m(wn)	part of total variance of the signal, at scale m, for a white noise process, Eq. (5)
f (Hz)	frequency
f_s (Hz)	sampling frequency of a signal
$f(t)$	signal to be investigated
m_j	wavelet scale (Fig. 2), defined by a frequency band $[f_s/2^{j+1}, f_s/2^j]$
M	largest resolvable scale in a discrete wavelet decomposition (determined by N)
N	number of data points in the signal treated
t (s)	time
$T_f(t,f)$	time–frequency representation of a signal $f(t)$

Greek symbols

Δf_i	uncertainty of the localization in the frequency domain (Fig. 2)
Δt_i	uncertainty of the localization in the time domain (Fig. 2)
ψ	basic wavelet function (mother wavelet), Eq. (1)

as a multiscale phenomenon with components on three distinct frequency scales [14]: low frequency components related to voids, medium frequency structures that represent particle clusters and high frequency elements associated with single particle motion. Wavelet analysis was also used by Chen et al. [15] for detection of singularities in the pressure signal. They applied the "wavelet transfer modulus maxima method" (WTMM, see ref. [16]) where the Lipschitz exponents of every maximum line (a line that connects points of the modulus maxima in the time–frequency space) were utilized to characterize the hydrodynamics of the bed (the transition between turbulent and fast fluidization was investigated). Roy et al. [17] proposed an algorithm for denoising the pressure signal obtained in a fluidized bed using a discrete wavelet transform. The major advantage of the method proposed is that a threshold level for the noise (a level below which all wavelet coefficients are either discarded or reduced) is identified automatically, i.e. not chosen a priori. Finally, Guo et al. [18] found that a bubble component of the pressure signal resided at a certain level of the wavelet representation. In summary, so far, wavelet analysis in the field of fluidization has been mostly focused on decomposing the signals into representative frequency ranges. On the other hand, the exceptional localization property of wavelets has not been significantly exploited.

This is the purpose of the present work that deals with a time–frequency representation (TFR) of three modes of bubble flow, classified in an earlier work [19]. That study looked into the interaction between a fluidized bed and its air-supply system. In the three modes, two types of bubbles were identified at different frequencies: the bubbles that produce pressure waves, which propagate throughout the entire system (air plenum, air-supply lines), and gaseous structures (exploding bubbles) in the bed, whose effects are not readily observed in the remainder of the system. Although nonstationarity of the signals treated is not a priori assumed, the presence of different dominant frequencies in the spectra makes it of interest to identify temporal localization of the underlying phenomena. In the present work, thus, the aim is to extract the more detailed information on the dynamics of the fluidization behaviour than obtained by classical Fourier analysis. For this purpose, first, the transient power spectral density analysis (van der Schaaf et al. [20]) is used as an indication of the presence of different frequencies in the time series at each instant of time. Then, discrete wavelet analysis is applied to illustrate the distribution of energy in the signals in the time–frequency plane and to calculate the fundamental time scales (defined as duration of a certain structure in the bed) of the major events that take place in the bed.

2. Theory

2.1. Transient spectral density analysis

Transient spectral density analysis is a simple technique, using standard Fourier methods, to observe whether the frequency composition in a certain signal changes in time. The procedure is as follows: the signal treated is divided into a number of segments and the power spectral density is calculated for each of them. The process results in a set of spectral densities as a function of time covering the entire time sequence. The outcome of the analysis is a surface plot with different colour intensities indicating the intensity of the power.

2.2. Wavelet analysis

A time–frequency representation (TFR) of a time series is a map of a one-dimensional signal in time $f(t)$, transformed mathematically into a two-dimensional function of time and frequency $T_f(t,f)$ (Fig. 1). In the time–frequency plane the horizontal axis spans the time domain of the signal (or its part), and the vertical axis ranges from zero to the Nyquist frequency. The values of the TFR surface covering the time–frequency plane indicate the spectral components present at given times. There are linear and quadratic TFRs. Although the quadratic structure of the TFR intuitively seems to be a reasonable assumption for the interpretation as a time–frequency energy distribution (since energy is a quadratic representation of the signal), the linear representations are by far more common in applied research. Among the latter, the short-time Fourier transform (or windowed Fourier transform) and the wavelet transform are mostly used. Contrary to the classical Fourier transform that provides a one-to-one relation between the time and frequency domains, the TFR combines

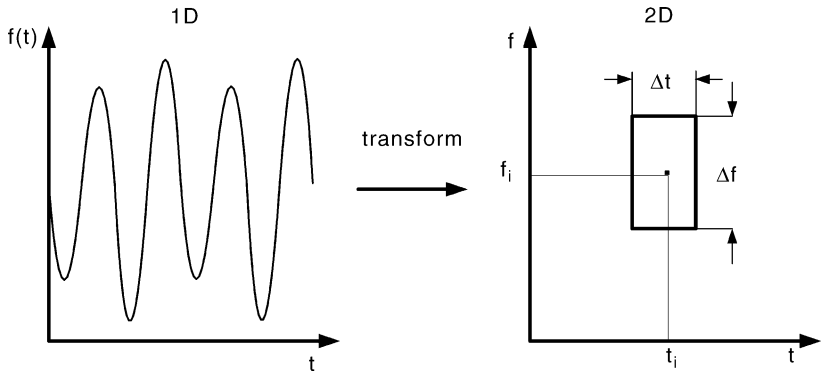

Fig. 1. Schematic time–frequency representation of a signal $f(t)$.f stands for frequency.

the two. Obviously, the information obtained by the Fourier transform is sufficient in a case of stationary signals as the frequency content of such signals does not change in time, and all frequency components exist all the time. However, if there is unsteadiness in the time series, it is of interest to extract possible local properties, both in time and frequency domain. The short-time Fourier transform uses a window of a constant length and the corresponding transform is computed for every part of a signal within each window (i.e. the signal is considered stationary within the chosen window). Wavelet transform is, on the other hand, regarded as a mathematical "microscope" [21] that is able to examine different parts of the time series by adjusting the focus of the "microscope". Because of this property, wavelet analysis will be applied in the present work.

The continuous wavelet transformation is defined [16] as the inner product of the analyzed signal $f(t)$ and the time-shifted and scaled version of a wavelet function Ψ:

$$CWf(a,b) = \langle f, \psi_{a,b}\rangle = \frac{1}{|a|^{1/2}} \int f(t)\psi^* \left(\frac{t-b}{a}\right) \mathrm{d}t \qquad (1)$$

Ψ (the star implies complex conjugate value) in Eq. (1) is called the mother wavelet and a and b are the dilation (scaling) and translation (location) parameters, respectively. The factor $1/|a|^{1/2}$ is a normalization factor. The "mother wavelet" must have two important properties [9]: a limited number of vanishing moments to allow time localization and a zero mean to facilitate reconstruction. The transform allows localization both in the time domain (via translations of the wavelet) and in the frequency domain (via dilatations of the wavelet). An important feature of the signal representation plane is that the uncertainties in the determination of time and frequency (the dimensions of the rectangles in the time–frequency plane (Fig. 2)) are not constant over the plane, but that their product is. This means that the uncertainties Δt_i and Δf_i, which localize a certain event in the time–frequency plane, cannot be made arbitrarily small at the same time. Towards high frequencies the time resolution improves at the expense of the frequency determination, whereas towards low frequencies the situation is the opposite. The concept of scales (m), presented in Fig. 2, is explained below.

To reduce computational cost, while maintaining the same degree of output information, the dilatation parameter (a) and the location parameter (b) in Eq. (1) are discretized. The procedure leads to a discrete wavelet transform, and by choosing the special case when the discretizations are proportional to each other ($a = a_0^m$; $b = nb_0a_0^m$), the following expression is obtained:

$$DWf(m,n) = \langle f, \psi_{m,n}\rangle = \frac{1}{|a_0|^{1/2}} \int f(t)\psi^*(a_0^{-m}t - nb_0)\mathrm{d}t \qquad (2)$$

Daubechies [22] has shown that for $a_0 = 2$ and $b_0 = 1$, an orthonormal family of functions (the condition imposed with the aim of minimizing the number of wavelet coefficients) may be constructed and that such a representation provides a multiresolution framework for analysis of phenomena present in a time series. In practise, the discrete wavelet transform is a pair of digital filters, which decompose a signal into a low frequency component A_1 (called the approximation) and a high frequency part D_1 (called the detail). In the next step, the approximation A_1 is used as an input, and by performing this operation recursively up to a level k, a hierarchical representation of the signal is obtained:

$$f(t) = \sum_{i=1}^{k} D_i + A_k \qquad (3)$$

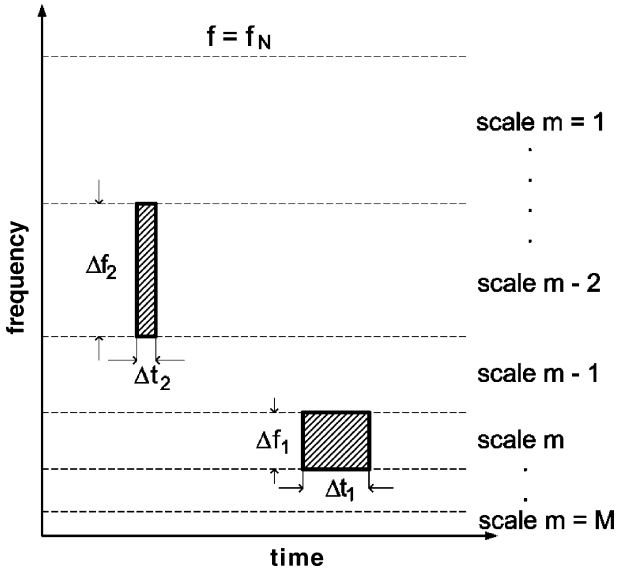

Fig. 2. Localization features in the time–frequency plane.

The detail D_i contains frequency information in the band $[f_s/2^{j+1}, f_s/2^j]$, where f_s is the sampling frequency and j is an integer. Each of these frequency bands defines a scale (denoted m (Fig. 2). At scale index 1, there are $N/2$ wavelet coefficients (N is the total number of data points in the signal), at index 2 there are $N/4$ and so on to the single coefficient at the final scale (determined as $m = \log 2(N)$ [16]). In summary, in the analysis presented, the scale is inversely proportional to the frequency of the classical Fourier analysis (every scale is spanned by a single period wave). Finally, the original signal can be reconstructed from wavelet coefficients by the inverse wavelet transform without loosing information [16].

It is important for the analysis of a certain event that the phenomenon studied falls exactly into one of the frequency bands. If not, the energy may spill over into the neighbouring bands, which makes the interpretation difficult. In such a case, a continuation of the wavelet transform called "wavelets packets" [23] should be used. They provide a more flexible and data-adaptive decomposition of a signal and are preferable, especially when high frequency phenomena are investigated (because of the poor frequency resolution of classical wavelet analysis at those frequencies). Another significant feature of the wavelets packets is that, unlike in classical wavelet analysis, scale is not inversely proportional to frequency, and every scale may be spanned by multiple period waves.

The present work primarily concerns low frequency phenomena and there is no need for "wavelets packets". The wavelets coefficients are interpreted statistically to illustrate that the classical wavelet transform is indeed sufficient for this study. Here, both antisymmetric ("Daubechies" as a representative class, see ref. [22]) and almost symmetric ("Sym" class [22]) wavelets are tested, since this particular property usually affects the outcome of a wavelet spectrum analysis [16].

The technique to identify different structures present in the time series from the orthogonal wavelet multiresolution analysis is to investigate the wavelet variance [24]. The results of such a statistical analysis may be compared with the ones obtained by classical Fourier analysis, since both bases are orthogonal. Also, conservation of energy, i.e. Parseval's identity, holds for wavelet coefficients (as it does in the Fourier analysis). The relative contribution of a structure (e.g. a bubble), captured by the detail D_i at scale m of a signal $f(t)$, to the total variance of the signal is defined as:

$$e_m = \frac{\sum_{i=1}^{2^{M-m}} \left(D_{sc}^{(m)}(i) \right)^2}{\sum_{j=1}^{M} \sum_{l=1}^{2^{M-j}} \left(D_{sc}^{(j)}(l) \right)^2} \tag{4}$$

with $m = 1, 2, \ldots M$ and $D_{sc}^{(m)}$ as the scaled wavelet coefficients, defined by $D_{sc}^{(m)} = 2^{m/2} D^{(m)}$. The general rule is that the more distinct a structure is, the more significant becomes the value of the squared wavelet coefficient at the particular location and scale. If an event (e.g. a bubble) may be unambiguously connected to a certain scale m, then it is straightforward to calculate its principal time scale (defined as the duration of the event in the bed). However, to do so, the resolution of the wavelet spectrum has to be high enough to clearly separate the scales. Usually an arbitrary threshold value is prescribed for the squared wavelet coefficients when an organized event is to be distinguished from the noise in the signal and coefficients smaller than the threshold are not taken into account. Since the choice of the threshold value introduces a certain degree of arbitrariness in the procedure, a different method is chosen in this work. The idea is that, at each scale, the data recorded are composed of an organized event and an accompanying white noise process. The more the data differ from the white noise, the more intense is the role of the structure identified at the corresponding scale. It is important to note that the maximum in e_m (Eq. (4)) does not necessarily secure the predominance of that individual scale in the signal. It is, namely, straightforward to show that the expectation of the energy of the white noise process is not equally distributed over the scales, but it can be written as [16]:

$$\langle e_m(\mathrm{wn}) \rangle = \frac{2^{M-m}}{2^M - 1} \tag{5}$$

where $m = 1, 2, \ldots M$. Eq. (5) shows that the expected value of the squared wavelet coefficients remains constant for each scale (M is constant for the data set investigated). This results in an exponential decay of e_m(wn) with the increase of m. Therefore, the relative significance of an organized event at each scale is obtained by plotting the difference between the total energy at that scale and the corresponding energy originating from white noise (e_m–e_m(wn)), versus the scale number m. The greater the difference, the more profound is the effect identified. At negative values the noise dominates the signal at the scale concerned.

3. Experiments

The data sets investigated were recorded by Sasic et al. [19] and experimental details are given in that work. Pressure fluctuations were measured in a unit, which is approximately scaled to model the dynamic behaviour of a 12 MWth circulating fluidized bed boiler [25]. However, during the investigation concerned, the unit was operated under noncirculating conditions, summarized in Table 1. Simultaneous measurements of pressure fluctuations in the bed and in the air plenum were performed. The bubble dynamics were studied by an optical probe, and the pressure fluctuations were measured (Honeywell pressure transducers, type 143PC03D) in the bed at the wall, 18 mm above the air distributor. The sampling frequency was 200 Hz, and the total amount of data acquired for each run was 48,000 points. The response time of the pressure sensor was low enough to

Table 1
Experimental and operating conditions

Temperature	Ambient
Cross section (m × m)	0.19 × 0.17
Height of the unit (m)	1.5
Bed material	Bronze
Particle diameter (mm)	0.10
Fluidization velocity (m/s)	0.18, 0.37, 0.73
Flux of solids (kg(m^2 s))	0 (bubbling conditions)
Air distributor pressure drop (Pa)	400, 520, 1000
Bed pressure drop (Pa)	2500

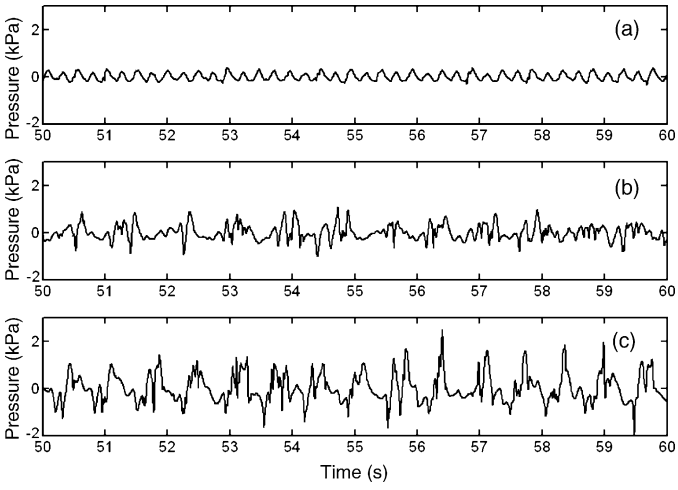

Fig. 3. Time sequences of pressure fluctuations in the bed in the three cases investigated: (a) $U = 0.18$ m/s; (b) $U = 0.37$ m/s; (c) $U = 0.73$ m/s.

capture the dynamics of the pressure fluctuations in the bed. The dimensions of the probe in combination with the transducer were proven not to distort the measurements, in agreement with van Ommen et al. [26].

4. Results and discussion

Pressure signals recorded in the bed in the three cases investigated are presented in Fig. 3 for a short interval of time. The signals differ significantly in amplitude, time scale and in overall shape. Fig. 4 illustrates the corresponding frequency spectra, each obtained as an average from a number of sub-spectra (the number being chosen to obtain a good trade-off between frequency resolution and statistical significance). The main features of the fluidization regimes that produced the spectra will be briefly outlined here; details are given in ref. [19]. At low fluidization velocity (0.18 m/s) and a pressure drop across the air distributor that is significantly lower than the pressure drop over the bed, a regime termed the single bubble regime is identified [27]. A piston-like movement of the bed as a whole and a strong periodicity in the formation and eruption of bubbles are observed. The cross section of the unit is large enough for slugging not to occur. After the eruption of a bubble, the bed collapses to a state free of bubbles (which leads to a discontinuity

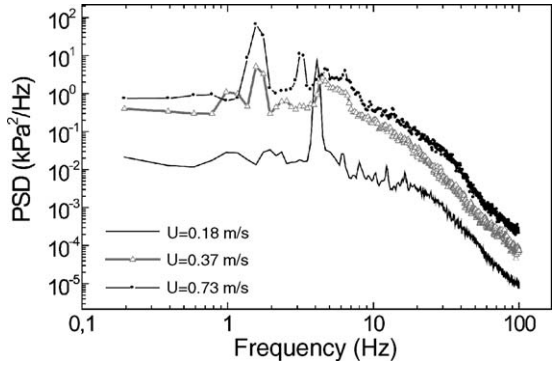

Fig. 4. Frequency spectra in the three cases investigated.

of the gas flow). The dominant frequency of the pressure signal measured in the bed fully coincides with the pressure variations identified in the air plenum and with the voidage recorded by an optical probe in the bed [19]. The explanation is [3,19] that after the collapse of the bed a pressure wave is created, which afterwards propagates throughout the entire system, given that the resistance of the air distributor is low. The fundamental frequency of such a bed can be described by a simple harmonic oscillator [27,28].

The character of fluidization becomes more complex when the gas velocity is increased to 0.37 m/s. A large number of small bubbles, growing rapidly in size, are observed above the air distributor. Fig. 4 shows that the pressure fluctuations in the bed have a peak at approximately 1.5 Hz (not seen at 0.18 m/s). The hypothesis that this peak represents so-called exploding bubbles [29] is confirmed by spectral analysis of the optical signal [19], showing that large voids of gas are present in the bed at the same frequency. Those voids may be conceived as shortcuts of gas from the air distributor through the bed into the splash zone, and no significant pressure wave is thereby created (the pressure peak at 1.5 Hz is not found in the air plenum [19]). On the other hand, the high frequency content of the signal in the bed is similar to that of the single bubble regime at 0.18 m/s, but with a somewhat wider frequency distribution. In summary, a complex flow field is established, consisting of large exploding bubbles and structures of small and intermediate size (bubbles related to pressure waves).

Finally, when the gas velocity is increased to 0.73 m/s, large structures below 2 Hz clearly dominate the signal recorded in the bed (Fig. 4). The high frequency content is still present and significant. The increased energy in the signal of the optical probe [19] indicates that the exploding bubbles grow in size as the gas velocity increases. Again, as in the 0.37 m/s case, the strong peak at 1.5 Hz is not found in the air plenum. Consequently, the bubbling behaviour of the bed may be separated into dominant gaseous structures (exploding bubbles) and bubbles related to pressure waves that propagate throughout the system (the higher frequency content (Fig. 4)). The waves are prevented from propagation only if the pressure drop over the distributor is large enough to decouple the bed from the rest of the system (this could take place at a pressure drop in the order of magnitude of the pressure drop over the bed or greater).

4.1. Transient spectral density analysis

Fig. 5 shows the outcome of the transient power spectral density analysis in the three cases investigated. The gray scale represents power and the vertical axis stands for frequency, while the horizontal axis shows the blocks into which the entire time series was divided. The spectral density was calculated for each block. In Fig. 5, eight blocks (30 s each) are chosen to obtain a fair trade-off between frequency resolution and statistical significance. In the single bubble regime only one single oscillation mode is present at approximately 4 Hz (Fig. 5a). The frequency content in that regime does not change; the dominant component exists all the time. On the other hand, in the complex regime, where pressure waves and exploding bubbles are competing

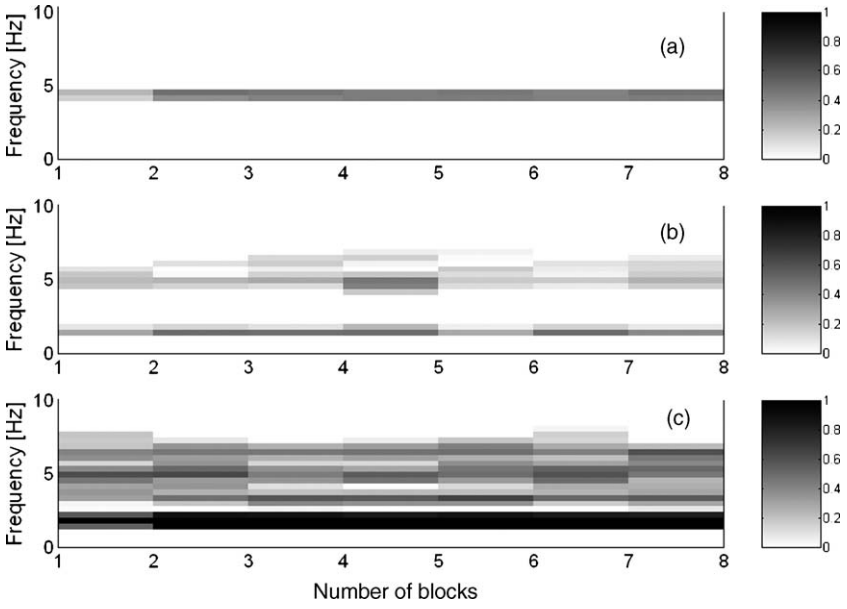

Fig. 5. Transient power spectral density in the three cases investigated: (a) $U = 0.18$ m/s; (b) $U = 0.37$ m/s; (c) $U = 0.73$ m/s.

effects (Fig. 5b), the power (the gray areas in the figure) does not remain constant throughout the signal. At a certain time one effect may dominate the flow field, whereas afterwards another takes over. Finally, Fig. 5c shows that at the highest velocity, the frequency component that represents large, exploding bubbles is present almost all the time in the signal, while the modes corresponding to pressure waves alternate between multiple frequency bands.

The simple analysis cannot provide any precise quantitative information on time localization of particular frequency components. However, it does indicate temporal changes in the oscillation mode of a certain fluidization regime, and thus, it points at the usefulness of more advanced methods.

4.2. Wavelet analysis

Fig. 6 illustrates the differences between the total energies (e) and the energies originating from white noise (e(wn)) at the corresponding scales m_i ($i = 1, 2 \ldots M$), using antisymmetric wavelets ("dB7" was used from the Daubechies class of wavelets. The wavelet of somewhat higher order was chosen, because regularity of a wavelet increases with the order. Decomposing the original signal using wavelets with increased regularity yields the smooth reconstructed signal, see ref. [22]). Close-to-symmetric wavelets were tested as well ("Sym4" from the symlets class), but little quantitative or qualitative difference was found. The dominant scales are readily observed in all cases treated, and furthermore, with sufficient scale resolution. Hence, Fig. 6a points at the existence of a dominant structure at scale $m = 5$. Having in mind the frequency range (3.1–6.2 Hz) that determines that scale with the sampling frequency used in the present work, and also conclusions from the previous work [19], shown in Fig. 4, the major structure is clearly identified as a single bubble present in the bed. Fig. 6b is equally revealing: at scale $m = 5$ the dominant effect is still present, but with somewhat less energy compared to the previous case. Another effect is seen at scale $m = 7$, corresponding to the previously identified exploding bubbles (Fig. 4). Also, the absence of any important effect at scale $m = 6$ is significant, which further proves the existence of a complex regime with two clearly defined and separated effects (pressure waves and exploding bubbles). Finally, Fig. 6c exemplifies the dominance of the exploding bubbles (which grow in size, since the energy at scale $m = 7$ is further increased compared to Fig. 6b). The diagram also shows that the impact of the pressure waves is now split over scales 5 and 6. The latter effect usually introduces problems in the interpretation of the results, but this is not the case in the present study, since it is credible to state that both scales represent pressure waves. The negative values at the vertical axes in Fig. 6 point towards the prevalence of noise (i.e. the lack of large, low frequency structures) in the signals investigated at the corresponding scales. Of course, the noisy component of the pressure signal recorded in fluidized beds is only approximately represented by white noise. Actually, there is a significant slope in the power spectrum, often modelled by a power-law [4]. Since the aim of the present work is the investigation of the low frequency phenomena, the exact nature of the noise is not of importance.

The results allow calculation of the duration of the structures identified in the bed. The duration of an event is defined as $2^{m+1}/f_s$ (s), i.e. it is twice as large as the actual wavelet scale that the structure belongs to. Using this reasoning, the duration of a single bubble in the bed is in the order of 0.3 s, whereas the exploding bubble lasts approximately 1.2 s. The time scale related to the pressure waves does not have the same physical meaning as in case of the other two structures. The waves, originating from phenomena in the bed are not limited to the bed only; they may be felt in the entire system (bed + air plenum + air-supply lines) and their propagation features are system dependant (the important parameters are: pressure drop at the air distributor, size of the air plenum, etc.).

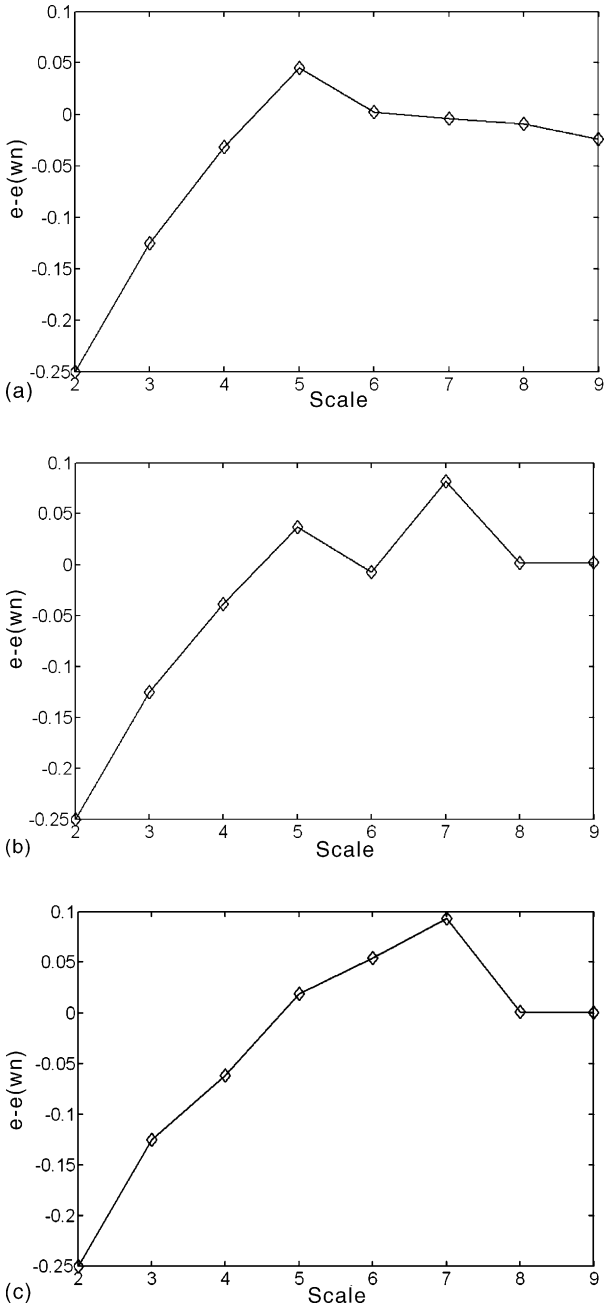

Fig. 6. Scalewise energy distribution in the pressure signal (antisymmetric wavelets ("dB7"): (a) $U = 0.18$ m/s; (b) $U = 0.37$ m/s; (c) $U = 0.73$ m/s.

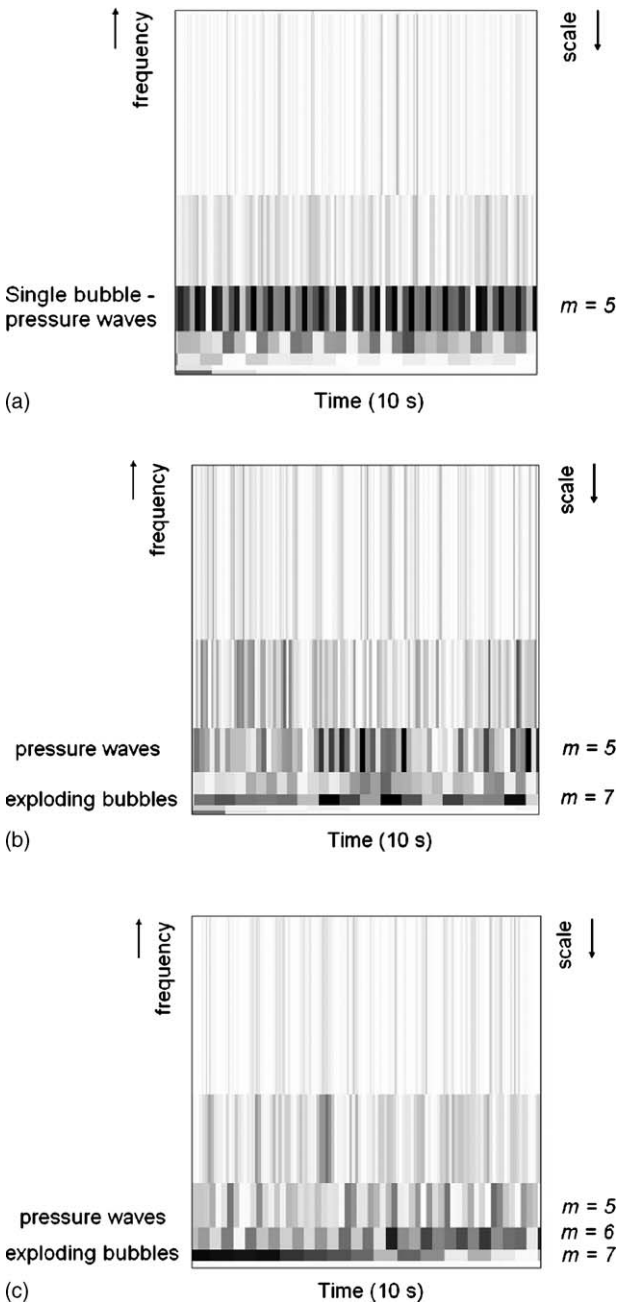

Fig. 7. Scalograms of the pressure fluctuation signals: (a) $U = 0.18$ m/s; (b) $U = 0.37$ m/s; (c) $U = 0.73$ m/s. Antisymmetric wavelets ("dB7") were used.

It is indicated above that wavelet decomposition is expected to separate the scales, while keeping the temporal reference. The qualitative outcome of such an analysis is a scalogram, i.e. a distribution of signal energy in the time–frequency (scale) plane. The scalogram is a visual two-dimensional representation of the signal, which illustrates the contribution of each pattern in the time-scale plane to the total energy of the signal. Such a representation is possible, since the wavelet coefficients are, in fact (see Eq. (1)), the correlation between the wavelet and a localized section of the signal treated. Consequently, if the signal has a significant frequency component corresponding to the given scale, the wavelet at this scale is close to the signal at that particular location, and the wavelet transform coefficient, obtained in that point, has a large value. Fig. 7a–c gives scalograms for the cases treated with the intensity of the gray-scale indicating the energy level of an individual cell (the cell in the time–frequency plane is defined by the uncertainties Δt_i and Δf_i (Fig. 2)). Thus, the higher the energy content of the cell, the darker is the cell in Fig. 7. For the sake of visual clarity only 10 s are shown on the time axis, and on the vertical axis, representing frequency (1/scale), the maximum is set to $f_N/4$ (f_N is the Nyquist frequency). As the gas velocity increases from 0.18 to 0.73 m/s, the cells corresponding to higher scales (lower frequencies) become more energetic. Fig. 7a, in accordance the statistical analysis of

the wavelet coefficients (Fig. 6a), clearly identifies scale $m = 5$ as the dominant one, and therefore, expresses the effect of the single bubbles present in the bed (which, in turn, produce pressure waves). In the same manner, Fig. 7b illustrates a complex flow field, consisting of pressure waves and exploding bubbles. Again, there is no significant structure at scale $m = 6$, i.e. the effect is identified with clear resolution. Finally, Fig. 7c shows the dominance of the exploding bubbles, as well as the split of the energy of the pressure waves into two neighbouring scales (5 and 6, with some energy present even at scale 4). However, the most important feature of Fig. 7 is that it provides a temporal localization of the phenomena identified, with by far superior resolution than in the transient power spectral density analysis (Fig. 5). It is seen that the single bubbles are evenly distributed in time (Fig. 7a), whereas Fig. 7b shows that the occurrence of the bubbles creating pressure waves is more irregular. In this fluidization regime (0.37 m/s), the distribution of the exploding bubbles in time is similar to the one of the pressure waves. In the highest velocity case (Fig. 7c), the irregularity of the occurrence of the exploding bubbles is demonstrated; a conclusion that somewhat differs from the one obtained from Fig. 5. The distribution of the bubbles responsible for pressure waves is similar to the one observed in the medium velocity case (Fig. 7b). Finally, it is important to have in mind that the temporal localization of the single bubbles and the pressure waves is obtained with higher resolution than for the exploding bubbles (due to the uncertainty principle (Fig. 2).

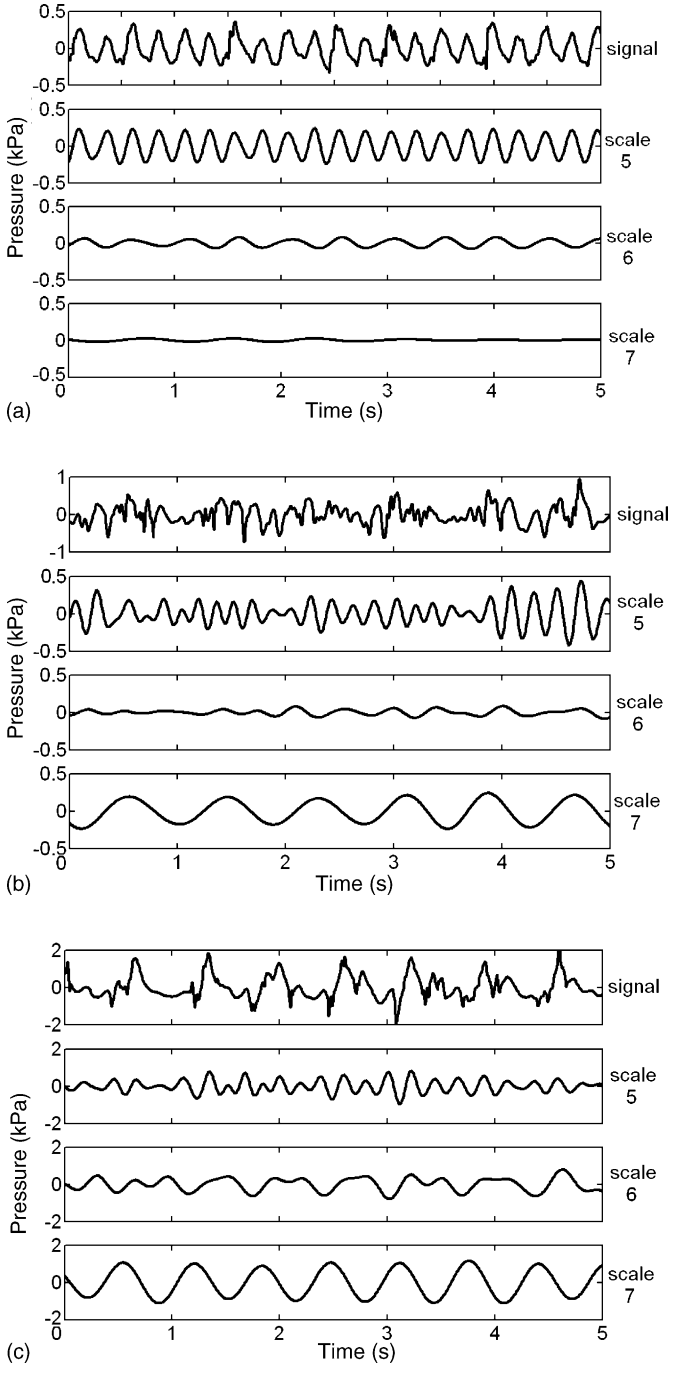

Fig. 8. Selected discrete wavelet transform coefficients (D5, D6 and D7) together with the original pressure signal: (a) $U = 0.18$ m/s; (b) $U = 0.37$ m/s; (c) $U = 0.73$ m/s.

Fig. 8a–c presents the original pressure signal in the three cases, together with the details, D5, D6 and D7, which have been shown to be of interest for the analysis in this work. It is obvious again that almost the entire energy in the low velocity case (Fig. 8a) resides in scale $m = 5$ (the same range in the vertical axis is kept for all signals to allow visual comparison). Consequently, this is another way to illustrate that the single bubbles are the main source of pressure fluctuations (and pressure waves as explained before) in this case. Furthermore, the number of peaks in scale $m = 5$ clearly fits into the major frequency of the classical Fourier analysis (Fig. 4). On the other hand, for the medium velocity case (Fig. 8b), significant energies are visible in scales 5 and 7, and so is the absence of important events in scale 6. The analysis of the number of peaks related to the respective scales unambiguously corresponds to the results presented in Fig. 4. The amplitude of the signals at scales 5 and 7 also shows that none of these effects is clearly dominant in the flow field. In the highest velocity case (Fig. 8c), the exploding bubbles are dominant in the bed (scale 7), with the number of peaks corresponding to the result from Fig. 4. Also, the widening of the frequency range of pressure waves is illustrated by the appearance of a signal with significant energy at scale 6.

5. Concluding remarks

Pressure signals recorded in a gas–solid fluidized bed have been analysed by wavelet and by transient spectral density analysis to assess the temporal properties of bed dynamics that are normally not captured by conventional frequency analysis, such as Fourier transform.

Transient spectral density analysis gives a simple, pictorial representation of the frequency composition of a signal in time. It was shown that, although no precise quantitative information was obtained on the time localization of the spectral components, temporal changes in the oscillation mode of the bed were qualitatively described.

Discrete wavelet decomposition expresses different frequency components (scales) in the signal and links them to the dynamic behaviour of a fluidized bed, in the present case,

to pressure fluctuations. By statistical analysis of calculated wavelets coefficients, bed phenomena, despite being complex, can be separated with high resolution in the time–frequency (scale) plane.

A model expresses the pressure signal recorded in a fluidized bed as comprised by an organized event (e.g. a bubble) and an accompanying white noise. This model uses the maximum difference between the energy of the signal at a given temporal location and scale and that of pure white noise to identify the time scale of dominant phenomena and their duration in the bed. It was shown that the type of wavelet base used for the analysis does not affect the results.

In addition, it is demonstrated that wavelet analysis represents not only an instrument for decomposing the signals into representative frequency bands, but it is also a powerful tool for the temporal localization of the phenomena of interest.

Wavelet analysis is valuable for the understanding of intrinsic features of pressure signals recorded in fluidized beds, but the use of wavelets is motivated only if they provide information that cannot be obtained by more common methods, such as classical Fourier analysis. An appropriate example is the study of localization in time of different phenomena identified in a signal.

Acknowledgement

This work was financed by the Swedish Energy Agency.

References

[1] R.C. Lirag, H. Litman, Statistical study of pressure fluctuations in a fluidized bed, AIChE Symp. Ser. 166 (67) (1971) 11–22.
[2] L.T. Fan, T.C. Ho, S. Hiraoka, W.P. Walawender, Pressure fluctuations in a fluidized bed, AIChE J. 27 (3) (1981) 388–396.
[3] A.P. Baskakov, V.G. Tuponogov, N.F. Filippovsky, A study of pressure fluctuations in a bubbling fluidized bed, Powder Technol. 45 (1986) 113–117.
[4] F. Johnsson, R.C. Zijerveld, J.C. Schouten, C.M. van den Bleek, B. Leckner, Characterization of fluidization regimes by time-series analysis of pressure fluctuations, Int. J. Multiphase Flow 26 (2000) 663–715.
[5] R. Brown, E. Brue, Resolving dynamical features of fluidized beds from pressure fluctuations, Powder Technol. 119 (2001) 68–80.
[6] J. Van der Schaaf, J.C. Schouten, F. Johnsson, C.M. van den Bleek, Non-intrusive determination of bubble and slug length scales in fluidized beds by decomposition of the power spectral density of pressure time series, Int. J. Multiphase Flow 28 (2002) 865–880.
[7] M.B. Priestley, Spectral Analysis and Time Series, Academic Press, London, 2001, ISBN 0-12-564922-3.
[8] Z. He, D. Zhang, B. Cheng, W. Zhang, Pressure-fluctuation analysis of a gas–solid fluidized bed using the Wigner distribution, AIChE J. 43 (2) (1997) 345–356.
[9] F. Hlawatsch, G.F. Boudreaux-Bartels, Linear and quadratic time–frequency signal representations, IEEE Signal Process. Mag. 9 (2) (1992) 21–67.
[10] I.M. Johnstone, B.W. Silverman, Wavelet threshold estimators for data with correlated noise, J. R. Stat. Soc. B 59 (2) (1997) 319–351.
[11] F. Argoul, G. Arneodo, G. Grasseau, Y. Gagne, E.J. Hopfinger, U. Frish, Wavelet analysis of turbulence reveals the multifractal nature of the Richardson cascade, Nature 338 (1989) 51–53.
[12] M. Farge, Wavelet transforms and their applications to turbulence, Annu. Rev. Fluid Mech. 24 (1992) 395–457.
[13] M. Antonini, M. Barlaud, P. Mathieu, I. Daubechies, Image coding using wavelet transform, IEEE Trans Image Process. 1 (2) (1992) 205–220.
[14] G.B. Zhao, Y.R. Yang, Multiscale resolution of fluidized-bed pressure fluctuations, AIChE J. 49 (4) (2003) 869–882.
[15] Y. Chen, Z. Tian, Z. Miao, Detection of singularities in the pressure fluctuations of circulating fluidized beds based on wavelet modulus maximum method, Chem. Eng. Sci. 59 (2004) 3569–3575.
[16] S. Mallat, A Wavelet Tour of Signal Processing, Academic Press, London, 1999, ISBN 0-12-466605-1.
[17] M. Roy, V.R. Kumar, B.D. Kulkarni, J. Sanderson, M. Rhodes, M. vander Stappen, Simple denoising algorithm using wavelet transform, AIChE J. 45 (11) (1999) 2461–2466.
[18] Q. Guo, G. Yue, T. Suda, J. Sato, Flow characteristics in a bubbling fluidized bed at elevated temperature, Chem. Eng. Process. 42 (2003) 439–447.
[19] S. Sasic, F. Johnsson, B. Leckner, Interaction between a fluidized bed and its air-supply system: some observations, Ind. Eng. Chem. Res. 43 (2004) 5730–5737.
[20] J. Van der Schaaf, J.C. Schouten, C.M. van den Bleek, F. Johsson, Multiple modes of bed mass oscillation in gas–solids fluidized beds, in: R.B. Reuther (Ed.), Proceedings of the 15th International Conference on Fluidized Bed Combustion, ASME, New York, Paper No. FBC99-0201, CD ROM, 1999.
[21] J. Drahos, M. Ruzicka, Problems of time series analysis in characterization of multiphase flows, in: Proceedings of the 5th International Conference on Multiphase Flow, ICMF '04' (2004) Yokohama, Japan, CD ROM, Paper No. K04, 2004.
[22] I. Daubechies, Ten Lectures on Wavelets, SIAM, Philadelphia, 1992.
[23] M.V. Wickerhauser, Lectures on Wavelets Packets Algorithms, Department of Mathematics, Washington University, St. Louis, 1991 (preprint).
[24] J. Poggie, A.J. Smits, Wavelet analysis of wall pressure fluctuations in a supersonic blunt-fin flow, AIAA J. 35 (10) (1997) 1597–1603.
[25] F. Johnsson, B. Leckner, A. Vrager, Solids flow pattern in the exit region of a CFB-furnace-influence of exit geometry, in: R.B. Reuther (Ed.), Proceedings of the 15th International Conference on Fluidized Bed Combustion, ASME, New York, Paper No. FBC99-0018 (CD ROM), 1999.
[26] J.R. van Ommen, J.C. Schouten, M.L.M. vander Stappen, C.M. van den Bleek, Response characteristics of probe-transducer systems for pressure measurements in gas–solid fluidized beds: how to prevent pitfalls in dynamics pressure measurements, Powder Technol. 106 (1999) 199–218.
[27] A. Svensson, F. Johnsson, B. Leckner, Fluidization regimes in non-slugging fluidized beds: the influence of pressure drop across the air distributor, Powder Technol. 86 (1996) 299–312.
[28] J.F. Davidson, First session - introduction by rapporteur, Inst. Chem. Eng. Symp. Ser. 30 (1968) 3–11.
[29] F. Johnsson, S. Andersson, B. Leckner, Expansion of a freely bubbling fluidized bed, Powder Technol. 68 (1991) 117–123.